The circumstellar envelope of S Sct

Groenewegen, M.A.T.; de Jong, T.

Publication date
1994

Published in
Astronomy & Astrophysics

[Link to publication](#)

The circumstellar envelope of S Scuti

M.A.T. Groenewegen[1] **and T. de Jong**[1,2]

[1] Astronomical Institute "Anton Pannekoek", Kruislaan 403, NL-1098 SJ Amsterdam, The Netherlands
[2] SRON, Laboratory for Space Research, P.O. Box 800, NL-9700 AV Groningen, The Netherlands

Abstract. We fit the observed spectral energy distribution (SED) of S Sct. This star is the only carbon star with a $60\,\mu$m excess mapped in detail in CO. For a distance of 460 pc, corresponding to a luminosity of $7050 L_\odot$, the CO data show that the present-day mass loss is low and that a phase of high mass loss ended about 9000 years ago. For the modelling of the SED we assume the following mass loss history: an initial mass loss rate ($\dot{M}_3$), followed by a phase of high mass loss ($\dot{M}_2$) lasting t_2 years, followed by a present-day mass loss rate ($\dot{M}_1$) lasting t_1 years. We consider both oxygen- and carbon-rich dust. The thickness of the CO shell implies a duration of the phase of high mass loss of between 350 and 1050 yr. The dust model allows values of t_2 up to 10^4 yr for some combination of parameters, indicating that the width of the shell observed in CO and the dust emission may be different. From the SED we derive an effective stellar temperature of $T_{\rm eff} = 2700$ K and $\dot{M}_1 = 5.5\,10^{-10} M_\odot$ yr^{-1}. The parameters t_1, t_2, $\dot{M}_2$ and $\dot{M}_3$ are determined from the IRAS 60 and 100 μm flux densities. Both oxygen- and carbon-rich models can be constructed that fit the SED. A value of $\dot{M}_3 = 8\,10^{-7} M_\odot$ yr^{-1} is estimated under the assumption that the duration of the phase of high mass loss is 1050 yr and ended 9000 yr ago. The mass lost during one thermal pulse cycle is estimated to be $\sim 0.08 M_\odot$. We predict that future (sub-)mm observations may resolve the question whether the dust which causes the 60 μm excess in carbon stars is carbon-rich or oxygen-rich. Taking into account the finite beam width of the IRAS detectors, reduces the time for stars with detached shells to describe a loop in the IRAS color-color diagram by $\sim$30% compared to earlier calculations. The best estimate for the loop time is $\sim 1.0\,10^4$ yr for oxygen-rich and $\sim 1.5\,10^4$ yr for carbon-rich dust shells.

Key words: stars: carbon – circumstellar matter – stars: evolution – stars: individual: S Sct – stars: mass loss

1. Introduction

The star S Sct belongs to the class of optically bright carbon stars with a $60\,\mu$m excess (Willems 1988). The chemi-

---

Send offprint requests to: M. Groenewegen

cal composition of the dust which causes this excess is still a matter of debate. Willems & de Jong (1988) suggested that these stars are formed after a thermal pulse has changed the previously oxygen-rich star into the present-day carbon star. The change in chemical composition of these stars could have caused the mass loss to drop and the oxygen-rich shell to expand and dilute, resulting in the 60 μm excess. This scenario has been criticized (see the discussion in Zuckerman & Maddalena 1989; de Jong 1989), the main concern being that it is still unproven that the detached shell is indeed oxygen-rich. Recently Zijlstra et al. (1992) showed that there are also M- and S-stars with a 60 μm excess. This implies that the drop in the mass loss rate probably takes place at some phase during most thermal pulses. Therefore, if a carbon star experiences another thermal pulse, which may also be accompanied by a temporary drop in the mass loss rate, the result could be a carbon star with a *carbon-rich* detached shell, which would also result in a 60 μm excess.

S Sct is the only carbon star with a 60 μm excess which has been mapped in detail in the CO line by Olofsson et al. (1992, hereafter OCEG) and Yamamura et al. (1993, hereafter YOKID). They derived the inner radius and thickness of the detached shell and estimated the mass loss history.

The aim of this paper is twofold. First of all, we use a dust radiative transfer code to fit the observed spectral energy distribution (SED). The parameters derived from the CO-modelling will act as constraints to the model. We investigate the possibility of discriminating between an oxygen-rich and a carbon-rich detached shell. Secondly, based on these fits to S Sct we investigate the time for stars with detached shells to describe a loop in the IRAS color–color diagram and compare the results to the earlier work of Willems & de Jong (1988) and Chan & Kwok (1988).

In Sect. 2 the CO results are summarised. In Sect. 3 the observed SED is presented and in Sect. 4 the radiative transfer model is outlined. In Sect. 5 the SED of S Sct is fitted and the results are discussed in Sect. 6.

2. The CO results

OCEG have mapped S Sct with the SEST. They found that the CO is distributed nearly spherically symmetric but is probably clumped. The present-day mass loss rate is low

and there is a geometrically thin (8″) shell at 68″ from the central star, expanding at 16.5 km s^{-1}. The mass in the shell is considerable ($\sim 0.04 M_\odot$), implying a phase of high mass loss in the past.

From OCEG we derive the following expressions. The mass loss rate which produced the shell is:

$$\dot{M}_{\rm shell} = 3.6\,10^{-5}\,(d/460)\,M_\odot\,{\rm yr}^{-1}\,, \qquad (1)$$

where d is the distance in pc. The uncertainty is a factor of 2. The phase of high mass loss ceased

$$t = 9000\,(d/460)\,{\rm yr} \qquad (2)$$

ago. This assumes an expansion velocity of 16.5 km s^{-1} and an inner radius of 68″. The geometrical extent (8″) of the shell implies a duration of the high mass loss of

$$\Delta t = 1050\,(d/460)\,{\rm yr}\,. \qquad (3)$$

The present-day mass loss is

$$\dot{M}_{\rm present} = 2.3\,10^{-8}\,(d/460)^2\,M_\odot\,{\rm yr}^{-1}\,. \qquad (4)$$

The uncertainty is a factor of 3. The present-day shell is expanding at roughly 5 km s^{-1}. Bergman et al. (1993) have modelled the CO data of OCEG in more detail. Their results do not differ significantly from the parameters derived by OCEG, which are used here.

After our work was completed we became aware of the results of YOKID. They observed the CO (1–0) line of S Sct with the Nobeyama telescope, which has a beam width of 16″ compared to the 44″ of the SEST. The spectra were fitted using a non-LTE molecular excitation code, taking into account chemical reactions and a self consistent temperature determination. The inner radius YOKID determine is within 2% of that of OCEG. They find expansion velocities of 16.5 and ~ 7 km s^{-1}, in good agreement with OCEG. The main difference is that YOKID derive a shell width 1/3 of that of OCEG, corresponding to $t_2 = 350$ yr in our model [see Sect. 5 and Eq. (3)]. In their modelling YOKID assume the CO to be uniformly distributed, while OCEG derive from their observations that the CO is clumped.

3. The observed spectral energy distribution

S Sct is a carbon star (number 4121 in Stephenson's 1989 catalog) with C/O = 1.07 and ^{12}C/^{13}C = 45 (Lambert et al. 1986). In Table 1 we present photometric data for S Sct collected from the literature. The observed flux densities are corrected for interstellar extinction adopting $A_V = 0.79$ and the interstellar extinction curve of Cardelli et al. (1989). The adopted value for A_V follows from the algorithm proposed by Milne & Aller (1980) and is consistent with the value of $0.6 \lesssim A_V \lesssim 0.9$ derived from Neckel & Klare

(1980). The IRAS flux densities in Table 1 are color-corrected. The integrated flux at earth is $1.07\,10^{-10}$ W m^{-2}. For an assumed luminosity of $7050 L_\odot$ (the observed mean luminosity of carbon stars in the LMC, Frogel et al. 1980) S Sct is at 460 pc. In Sect. 5 the predicted model flux densities are directly compared to the observed IRAS flux densities in the PSC: $S_{12} = 58.3 \pm 7.8$ Jy, $S_{25} = 17.3 \pm 1.4$ Jy, $S_{60} = 9.3 \pm 1.1$ Jy and $S_{100} = 14.1 \pm 1.7$ Jy.

S Sct is classified as an SRb variable with a period of 148 d (Kholopov et al. 1985). The amplitude of the variability is small. The standard deviation in the Geneva photometric system (Rufener 1988) is only 0.13 mag in the V-band. The IRAS variability index is 0.

There is no LRS-spectrum in the LRS atlas (Joint IRAS Science Working Group 1986) but Volk & Cohen (1989) have extracted the spectrum from the LRS database. The spectrum is noisy but is essentially featureless and does not show the silicate or the silicon carbide feature. This implies a low present-day mass loss rate.
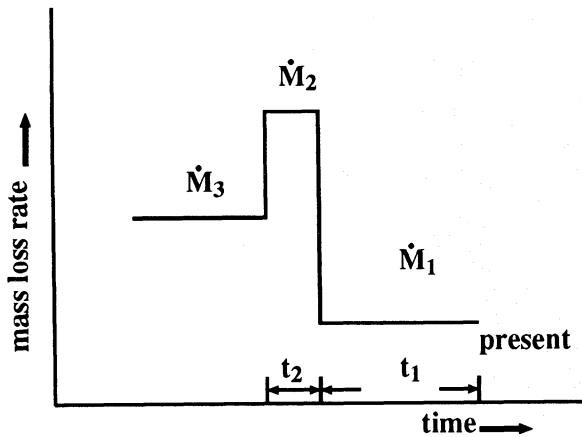
4. The dust radiative transfer model

The dust radiative transfer model of Groenewegen (1993) is used. This model was developed to handle non-r^{-2} density distributions. It simultaneously solves the radiative transfer equation and the thermal balance equation for the dust. The adopted mass loss history is schematically illustrated in Fig. 1. The central star is represented by a blackbody of temperature $T_{\rm eff}$. For the carbon-rich dust we assume amorphous carbon. The absorption coefficient is calculated from the optical constants listed in Rouleau & Martin (1991) for the AC1-amorphous carbon species. For the oxygen-rich dust we assume astronomical silicate (Draine & Lee 1984; Draine 1987). Condensation temperatures are 1500 and 1000 K respectively. For both the carbon- and oxygen-rich dust we assume a dust-to-gas ratio of $\Psi = 0.01$, a grain radius $a = 0.03\,\mu$m and a grain density $\rho = 2.0$ g cm^{-3}. The expansion velocity in phase 2 is 16.5 km s^{-1}. For convenience we assumed the same expansion velocity in phases 1 and 3. This seems inconsistent with the observed present-day (phase 1) velocity of about 5 km s^{-1}, which implies that there may be a gap between the expanding shell and the matter currently expelled with a lower velocity. The density distribution may therefore be more complicated than sketched in Fig. 1. We verified that the neglect of the possible gap has negligible influence on the predicted flux densities (less than 0.015 Jy).

It is conceivable that the expansion velocity in phase 3 were less than 16.5 km s^{-1}. In that case the expanding shell would have swept up matter. This effect is negligible since the amount of matter swept up in 10 000 yr is $\sim 2\,10^{-3}M_\odot$ (for a mass loss rate and an expansion velocity in phase 3 of $10^{-7}M_\odot$ yr^{-1} and 5 km s^{-1} respectively) which is much smaller than the mass in the shell ($\sim 0.04 M_\odot$). The outer radius is determined in the model by a dust temperature of 20 K and scattering is neglected.

Table 1. The observed fluxes of S Sct

Reference	$\lambda\,(\mu m)$	$F_\lambda\,(W\,m^{-2}\,\mu m^{-1})$	Reference	$\lambda\,(\mu m)$	$F_\lambda\,(W\,m^{-2}\,\mu m^{-1})$
Rufener (1988)	0.346	6.39 (−15)	Walker (1980)	1.25	5.00 (−10)
	0.402	8.48 (−13)		1.65	3.88 (−10)
	0.448	3.65 (−12)		2.20	2.41 (−10)
	0.540	4.51 (−11)		3.5	6.73 (−11)
	0.549	6.11 (−11)			
	0.581	8.29 (−11)	Hackwell (1972)	2.3	2.50 (−10)
				3.5	9.37 (−11)
Walker (1979)	0.360	8.52 (−14)		4.8	1.52 (−11)
	0.440	5.56 (−12)		8.6	2.40 (−11)
	0.550	6.39 (−11)		10.8	2.44 (−12)
	0.640	1.40 (−10)			
	0.790	2.71 (−10)	Gillet et al. (1971)	3.5	5.91 (−11)
				4.9	1.13 (−11)
Šleivyté (1987)	0.405	3.4 (−13)		8.4	2.81 (−12)
	0.466	9.3 (−12)		11.0	1.27 (−12)
	0.516	3.03 (−11)			
	0.544	5.04 (−11)	Ney & Merrill (1980)	3.5	5.91 (−11)
	0.655	1.70 (−10)		4.9	1.14 (−11)
				8.4	3.37 (−12)
Noguchi et al. (1981)	1.00	4.91 (−10)		11.2	1.10 (−12)
	1.25	4.80 (−10)			
	1.65	4.14 (−10)	Price & Murdock (1983)	4.2	3.95 (−11)
	2.25	2.40 (−11)		11.0	1.90 (−12)
	3.12	7.78 (−11)			
	3.70	6.74 (−11)	IRAS PSC	12	9.76 (−13)
			color-corrected	25	5.99 (−14)
				60	8.39 (−15)
				100	4.23 (−15)

Fig. 1. The adopted schematic mass loss history

A feature which is usually neglected in radiative transfer calculations is the finite beam size of the IRAS detectors. In a star not surrounded by a detached shell this effect is probably not very important but considering that the emission of S Sct arises from dust at 1′ from the star this effect could be significant. The information on the spatial response of the IRAS detectors was taken from Table II.C.3, Table IV.A.1

and Fig. IV.A.3 of the *Explanatory Supplement* (Joint IRAS Science Working Group 1986). The 12 and 25 μm beams are taken to be rectangular with FWHM values of 60″ in the in-scan direction for both detectors. The 60 and 100 μm beams are taken to be Gaussian with in-scan FWHM values of 120″ and 220″ respectively. For $\lambda > 140\,\mu$m we assume a Gaussian beam with FWHM = 18.5″. This approximates the beam size of the JCMT telescope at mm-wavelengths and allows us to estimate (Sect. 6) the flux which would be measured by the UKT 14 instrument (Duncan et al. 1990).

In the models the calculated flux is convolved with the spectral response (Table II.C.5 of the *Explanatory Supplement*) to compare the predicted fluxes directly to the fluxes listed in the PSC. A model is found to be in agreement with observations if the predicted flux densities are within the flux uncertainty of the observed flux densities.

For an easy interpretation of the model results it is useful to derive some analytical relations for the dust emission in the case that the emission is optically thin at all wavelengths. In the optically thin case and with an absorption coefficient $Q_\lambda \sim \lambda^{-p}$ the inner radius of the dust shell varies like $r_c \sim (T_{\rm eff}/T_c)^{(4+p)/2}$, where T_c is the (condensation) temperature at the inner radius. For carbon-rich dust

we find from our models:

$$r_c (\text{in } R_*) = 2.313 \left(\frac{T_{\text{eff}}}{2700} \frac{1500}{T_c} \right)^{2.45} . \tag{5}$$

The exponent is very close to the expected value of 2.5 for carbon-rich dust ($p = 1$). The emission (per unit wavelength) at infrared wavelengths is given by

$$S(\lambda) = S_*(\lambda) + \Delta S(\lambda), \tag{6}$$

where S_* is the contribution from the central star and ΔS represents the dust emission. The stellar contribution can be written as:

$$S_*(\lambda) = \frac{B_\lambda(T_{\text{eff}})}{T_{\text{eff}}^4} \frac{L}{4\sigma d^2} , \tag{7}$$

where L is the luminosity of the star and σ is the Stefan–Boltzmann constant. In the optically thin case the dust emission in the shell is given by (Sopka et al. 1985)

$$\Delta S(\lambda) = \frac{\pi a^2 Q_\lambda}{4\pi d^2} \int_{r_{\text{inner}}}^{r_{\text{outer}}} B_\lambda[T(r)]n(r)4\pi r^2 \, dr , \tag{8}$$

where $n(r)$ is the dust grain number density and $T(r)$ the dust temperature profile. The optical depth is defined as

$$\tau_\lambda = \int_{r_c}^{\infty} \pi a^2 Q_\lambda n(r) \, dr = \frac{3\dot{M}\Psi Q_\lambda/a}{16\pi r_c R_* v \rho} , \tag{9}$$

where Ψ is the dust-to-gas ratio, a the grain radius, ρ the grain density, r_c the inner radius in units of stellar radii and R_* the stellar radius in cm. The last equality in Eq. (9) assumes a $1/r^2$ density distribution. Equation (8), with the help of Eq. (9) can be written as

$$\Delta S(\lambda) = \tau_\lambda \frac{(r_c R_*)^2}{d^2} \left(\frac{\lambda k T_c}{hc} \right)^{(4+p)/2} \frac{hc^2(4+p)}{\lambda^5}$$

$$\times \int_{hc/\lambda k T_c}^{\infty} \frac{y^{1+p/2}}{\exp(y) - 1} \, dy . \tag{10}$$

The integral is only weakly dependent on T_c. For example, when $p = 2$ and $\lambda = 12 \, \mu$m the integral changes by 8.5% when T_c is varied from 1500 to 1000 K. At longer wavelengths the T_c dependence of the integral is even less.

5. Results

5.1. The effective temperature and the present-day mass loss

The effective temperature and the present-day mass loss can be constrained without considering the 60 and 100 μm fluxes. For example, an effective temperature less than 2500 K can be excluded because this results in $S_*(25) > 18.7$ Jy. When T_{eff} is increased beyond 2500 K the stellar flux decreases at infrared wavelengths and there is increasing room for dust emission. For high effective temperatures

the spectrum peaks at shorter wavelengths which for $T_{\text{eff}} \gtrsim 3000$ K is no longer in agreement with the observed SED. We determined the effective temperature and the present-day mass loss rate by fitting the SED up to 25 μm. It turns out that it is not possible to fit the UV part of the spectrum ($\lambda < 0.5 \, \mu$m) for any reasonable effective temperature. This is probably due to the blackbody approximation for the stellar flux which does not take into account the effect of molecular absorption bands. An effective temperature of 2700 K gives a good fit from 0.5 to 25 μm. Lambert et al. (1986) quote $T_{\text{eff}} = 2895$ K based on the infrared-flux method.[1]

The present-day mass loss rate is determined by fitting the 12 and 25 μm points. For carbon-rich dust and a mass loss rate of $\dot{M}_1 = 5.5 \, 10^{-10} M_\odot \, \text{yr}^{-1}$ the model has 12 and 25 μm fluxes of 66.9 and 17.3 Jy, in excellent agreement with observations. The present-day mass loss rate we derive is considerably less than that estimated from the CO. It is unclear how to explain this. As mentioned in Sect. 3 the LRS spectrum is photospheric showing no dust emission features. May be the estimate from the CO is too high. OCEG have derived the present-day mass loss rate from the Knapp & Morris (1985) formula which is based on the kinetic temperature of IRC 10216. This most certainly is not applicable in the case of S Sct. For our model we adopt an effective temperature of $T_{\text{eff}} = 2700$ K and a present-day mass loss rate of $5.5 \, 10^{-10} M_\odot \, \text{yr}^{-1}$ which results in $S_*(60) = 2.88$ Jy and $S_*(100) = 0.87$ Jy when folded with the IRAS spectral response.

5.2. The mass loss history

The far-infrared fluxes are determined by the parameters t_1, t_2, $\dot{M}_2$ and $\dot{M}_3$. We calculated several models to illustrate the influence of the parameters. Results for carbon-rich and oxygen-rich detached shells are collected in Tables 2 and 3. Based on the analysis of the CO observations (Sect. 2) the value of t_1 is initially fixed at 9000 yr and the mass loss rate in phase 3 is arbitrarily set at 1% of $\dot{M}_2$. For the duration t_2 of mass loss phase 2 we adopt different values: 350 yr (see YOKID), 1050 yr (see OCEG), 3050 yr (the best fit) and 14050 yr (the maximum value allowed by the IRAS data) for the carbon-rich shell. For the oxygen-rich shell values of $t_2 = 350$, 1050 and 2450 yr are considered. For $t_2 = 350$ and 1050 yr we determined the value of t_1 that best fits the IRAS 60 and 100 μm fluxes and found $t_1 \approx 9700$ for the carbon-rich and ≈ 7700 yr for the oxygen-rich shell. For $t_2 = 1050$ the range in t_1 and $\dot{M}_2$ allowed by the IRAS data is 8000–11500 yr and 1.7–$4.2 \, 10^{-5} M_\odot \, \text{yr}^{-1}$ for the carbon-rich shell and

---

[1] In the YOKID paper an effective temperature of 2350 K is assumed in their radiative transfer model. Although their calculated spectrum nicely fits the few data points in their plot, such a low effective temperature can be excluded on the basis of the larger observational data set listed in Table 1.
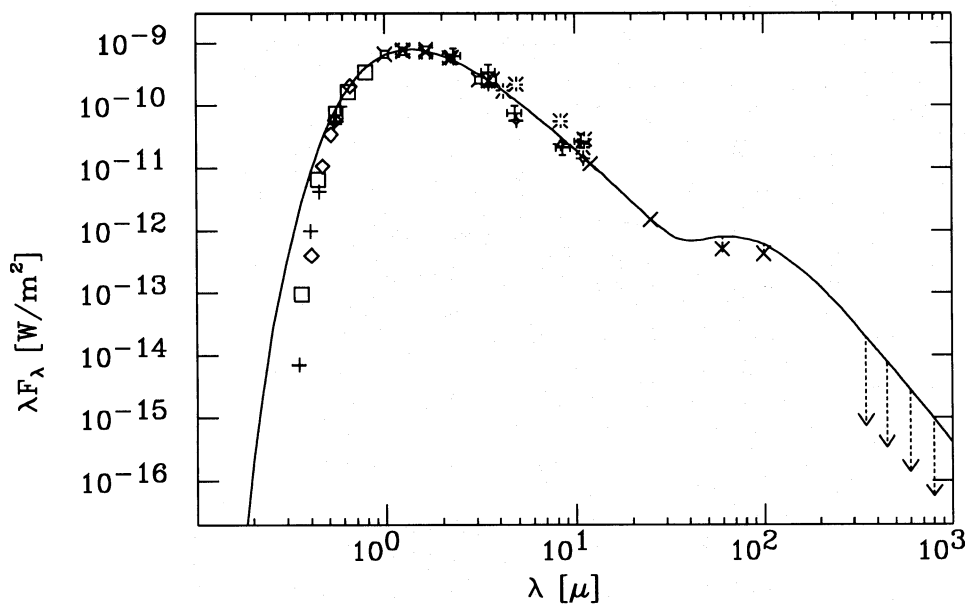
Fig. 2. The observed spectral energy distribution of S Sct compared to the carbon-rich model with $t_1 = 9735$ yr and $t_2 = 1050$ yr. The effective temperature and present-day mass loss rate are 2700 K and $5.5\ 10^{-10} M_\odot$ yr^{-1}, respectively. The symbols indicate different sources of photometry (see Table 1): X = IRAS, + = Rufener (1988), $\diamond$ = Šleivyté (1987), $\square$ = Walker (1979), $\diamondsuit$ = Gillet et al. (1971), $\bowtie$ = Noguchi et al. (1981), $\ddagger$ = Hackwell (1972), $\times$ = Walker (1980), $*$ = Ney & Merrill (1980) and Price & Murdock (1983). The solid line is the model without beam effects. The dashed line with arrows indicate the beam effect of IRAS observations (at 60 and 100 μm) and the JCMT (at 350, 450, 600 and 800 μm). The beam effect at (sub-) mm wavelengths is so large that only the central star is observed

6000–9500 yr and 3.8–$12\ 10^{-5} M_\odot$ yr^{-1} for the oxygen-rich shell, respectively. For the carbon-rich model with $t_1 = 9000$ and $t_2 = 1050$ we investigated the influence of the ratio $\dot{M}_2/\dot{M}_3$. A best fit is found for a ratio of ~ 13. No fit is found for the oxygen-rich shell. An example of the fits is shown in Fig. 2 for the carbon-rich model with $t_1 = 9735$ and $t_2 = 1050$ yr. The results are further discussed in Sect. 6.

Our conclusion may be affected by cirrus since S Sct is located at only 3 degrees below the galactic equator. The PSC lists a CIRR-2 index of 5, suggesting that up to 30% of the 100 μm flux may be due to cirrus, although Egan & Leung (1991) concluded that cirrus is not a major factor in determining the 60/100 color in carbon stars. To investigate the possible influence of cirrus contamination we assume that the true flux from S Sct at 60 and 100 μm is 70% of the flux listed in the PSC. With the help of Eqs. (6) and (10) and the stellar fluxes listed in Sect. 3 a new set of best-fitting parameters can be estimated (last entry in Tables 2 and 3). Cirrus contamination does not alter our conclusion that both oxygen-rich and carbon-rich models are consistent with the IRAS data. However, the best fitting oxygen-rich model is in better agreement with the IRAS data than the best-fitting carbon-rich model.

In the models, specific values are adopted for the expansion velocity, the dust condensation temperature, the effective temperature and the distance (c.q. luminosity). To indicate how the derived mass loss rates and time scales depend on these parameters we use the equations in Sect. 4. The dependence on the distance and the expansion velocity is like $t \sim d/v$ and $\dot{M} \sim vd$ [cf. Eq. (9)]. We next investigate the dependence on the condensation temperature and the effective temperature. From Eqs. (5), (9) and (10) it follows that $\Delta S \sim f(T_c)T_{eff}^{0.5}$, where $f(T_c)$ denotes the integral in Eq. (10). Since $f(T_c)$ is only weakly dependent on the condensation temperature, the dependence of the mass loss rates and time scales on T_c is weak. The effect of the effective temperature is more complicated, since both the stellar and the dust contribution are changed. When the effective temperature is increased, the stellar flux at infrared wavelengths is decreased while the dust emission is increased. From comparison with a model with $T_{eff} = 2800$ K we find that the effects of the stellar and the dust contribution nearly cancel.

6. Discussion and conclusion

Although the models for oxygen- and carbon-rich shells in Tables 2 and 3 are formally in agreement with the SED, the best carbon-rich model is in better agreement with the IRAS data then the best oxygen-rich model. We find $t_1 = 9735$ yr, $\dot{M}_2 = 2.7\ 10^{-5} M_\odot$ yr^{-1} for the carbon-rich model and $t_1 = 7620$ yr, $\dot{M}_2 = 7.0\ 10^{-5} M_\odot$ yr^{-1} for the oxygen-rich model. The values derived from the CO observations are $t_1 = 9000$ yr and $\dot{M}_2 = 3.6\ 10^{-5} M_\odot$ yr^{-1}. The mass loss rates are uncertain to a factor of ~ 5 due to uncertainties in the dust-to-gas ratio and the absolute value of Q_λ but the time scales are determined accurately. Since the expansion velocity is known the major uncertainty is in the adopted luminosity. The lifetimes scale like $\sqrt{L}$.

Since the CO shell in the high mass loss phase may be partially or largely destroyed by photodissociation the dust shell may be much ticker than the CO shell. The duration

Table 2. Results for a carbon-rich detached shell

t_1 (yr)	t_2 (yr)	$\dot{M}_2(M_\odot \, \mathrm{yr}^{-1})$	$\dot{M}_3(M_\odot \, \mathrm{yr}^{-1})$	S_{60} (Jy)	S_{100} (Jy)
9000	350	$5.24 \, 10^{-5}$	$5.24 \, 10^{-7}$	9.28	12.74
9000	1050	$1.94 \, 10^{-5}$	$1.94 \, 10^{-7}$	9.28	12.80
9000	3050	$9.51 \, 10^{-6}$	$9.51 \, 10^{-8}$	9.28	14.12
9000	14050	$5.00 \, 10^{-6}$	$5.00 \, 10^{-8}$	8.32	15.78
9730	350	$7.34 \, 10^{-5}$	$7.34 \, 10^{-7}$	9.28	14.11
9735	1050	$2.69 \, 10^{-5}$	$2.69 \, 10^{-7}$	9.28	14.11
9000	1050	$1.65 \, 10^{-5}$	$1.3 \, 10^{-6}$	9.28	14.11
11000	1050	$2.4 \, 10^{-5}$	$2.4 \, 10^{-7}$	6.50	9.88

Table 3. Results for an oxygen-rich detached shell

t_1 (yr)	t_2 (yr)	$\dot{M}_2(M_\odot \, \mathrm{yr}^{-1})$	$\dot{M}_3(M_\odot \, \mathrm{yr}^{-1})$	S_{60} (Jy)	S_{100} (Jy)
9000	350	$25.6 \, 10^{-5}$	$25.6 \, 10^{-7}$	8.84	15.80
9000	1050	$10.7 \, 10^{-5}$	$10.7 \, 10^{-7}$	8.69	15.78
9000	2450	$5.30 \, 10^{-5}$	$5.30 \, 10^{-7}$	8.28	15.79
7750	350	$1.72 \, 10^{-4}$	$1.72 \, 10^{-6}$	9.28	14.11
7620	1050	$7.00 \, 10^{-5}$	$7.00 \, 10^{-7}$	9.28	14.12
8800	1050	$6.0 \, 10^{-5}$	$6.0 \, 10^{-7}$	6.50	9.88

of the high mass loss phase is constrained by the infrared observations. For $t_1 = 9000 \, \mathrm{yr}$ we find that $t_2 = 2450$ and $14\,050 \, \mathrm{yr}$ are just compatible with the IRAS observations in the case of an oxygen- and a carbon-rich shell respectively.

Suppose that a negligible amount of the CO associated with phase 2 has been dissociated. This implies that the value of t_2 derived from the CO observations is the true duration of the phase of high mass loss. A lifetime of 1050 yr for phase 2 is consistent with theoretical estimates which indicate that the duration of the increase in luminosity after a TP is about 1% of the interpulse time. Recent calculations by Vassiliadis & Wood (1993) show that the interpulse period is between $5 \, 10^4$ and $10^5 \, \mathrm{yr}$. This implies theoretical values for t_2 of 500–1000 yr. Using the CO data as constraint allows an estimate for the mass loss rate in phase 3. With t_1 and t_2 fixed at 9000 and 1050 yr we determined $\dot{M}_2$ and $\dot{M}_3$ that best fit the IRAS data (see Table 2). The derived value of $\dot{M}_3$ scales with v_3. The value of v_3 is not known but is very likely to be in between the observed expansion velocities in phases 1 ($v_1 \approx 5 \, \mathrm{km \, s}^{-1}$) and 2 ($v_2 = 16.5 \, \mathrm{km \, s}^{-1}$). If $v_3 = 10 \, \mathrm{km \, s}^{-1}$ then $\dot{M}_3 = 8 \, 10^{-7} M_\odot \, \mathrm{yr}^{-1}$. For an oxygen-rich shell no satisfactory model exists.

With values for the mass loss rates during the differ-ent phases of the thermal pulse cycle one can estimate the total mass lost. The observed duration of the thermal pulse (associated with the phase of high mass loss) of 1050 yr suggest that the interpulse period was $10^5 \, \mathrm{yr}$ (see Vassiliadis & Wood 1993). An appropriate lifetime for the luminosity dip is then $\sim 2 \, 10^4 \, \mathrm{yr}$. The mass lost during the thermal pulse is $1050 \, \mathrm{yr} \, \star 1.65 \, 10^{-5} M_\odot \, \mathrm{yr}^{-1} \approx 0.02 M_\odot$. The mass lost during the luminosity dip is very small $2 \, 10^4 \, \mathrm{yr} \, \star 2.3 \, 10^{-8} M_\odot \, \mathrm{yr}^{-1} \approx 4 \, 10^{-4} M_\odot$. The mass lost during the quiescent H-shell burning phase is $8 \, 10^4 \, \mathrm{yr} \, \star 8 \, 10^{-7} M_\odot \, \mathrm{yr}^{-1} \approx 0.06 M_\odot$. This shows that most mass is lost in the quiescent phase. The total mass lost over one pulse cycle is $0.08 M_\odot$. The average mass loss rate over the pulse cycle is about $8 \, 10^{-7} M_\odot \, \mathrm{yr}^{-1}$. The mass lost in the phase of high mass loss derived from our dust modelling is a factor of 2 lower than that deduced from the CO. Considering the factor of 2 uncertainty in the CO result and the factor of 5 uncertainty in our result the two values are consistent.

Could future sub-mm continuum observations distinguish between a carbon-rich and an oxygen-rich shell? For selected models we calculate the flux-densities expected for the UKT 14 instrument at the JCMT at 850 and 1100 μm.

Table 4. Predicted KAO and JCMT flux densities at 100, 850 and 1100 μm

Grain type	t_1 (yr)	t_2 (yr)	JCMT on source		JCMT off source		KAO on source
			850 μm (mJy)	1100 μm (mJy)	850 μm (mJy)	1100 μm (mJy)	100 μm (Jy)
Carbon	9000	1050	13.2	7.6	2.20	0.91	1.36
Carbon	9000	14050	13.4	7.7	2.37	1.08	1.29
Carbon	9735	1050	13.3	7.7	2.89	1.31	1.35
Oxygen	9000	1050	12.3	7.1	1.14	0.40	1.46
Oxygen	9000	2450	12.3	7.1	1.29	0.45	1.41
Oxygen	7620	1050	12.3	7.1	0.29	0.099	1.56

Table 5. The time to reach $C_{32} = -1.55$ after the mass loss stops

Grain type	Beam effect	t (yr)	Grain type	Beam effect	t (yr)
Oxygen	With	12 400	Carbon	With	16 100
Oxygen	Without	16 400	Carbon	Without	23 300

A Gaussian beam with a FWHM value of 18.5″ is assumed. Both the on-source flux density and the flux density at 72″ (i.e. 68″ inner radius plus half the shell width) from the central star are determined. The predicted flux densities are listed in Table 4. The on-source flux density is higher than the off-source flux density but the differences between the different models are too small to be observationally significant. The beam of the JCMT is much smaller than the inner radius of the shell so only the central star is measured. It is better to observe the circumstellar shell directly. Not only have the carbon-rich models higher off-source flux densities than the oxygen-rich models, the spectral index ($S_\nu \sim \lambda^{-\alpha}$, with $\alpha \approx 3$ for the carbon-rich models and $\alpha \approx 4$ for the oxygen-rich models) is significantly different. Unfortunately, the predicted flux densities are too low to be measured accurately enough with the UKT14 instrument.[2] The flux densities will be within the reach of the next generation of JCMT instruments, e.g. the Sub-millimeter Common User Bolometer Array (SCUBA).

Hawkins (1992) has measured the on-source 100 μm flux density of S Sct onboard the Kuiper Airborne Observatory with a FWHM = 30″ beam. He finds a 3σ upper limit of 3 Jy. In the last column of Table 4 we predict the on-source 100 μm flux density for different models for a 30″ beam. We find $S_{100} < 1.6$ Jy, consistent with Hawkins upper limit.

Having determined the parameters characterizing the present status of S Sct, we are able to calculate the evolution of the spectral energy distribution. This is done for carbon-rich and oxygen-rich shells, and with and without the effect of the finite IRAS beams. The latter makes a comparison possible with the calculations of Willems & de Jong (1988) and Chan & Kwok (1988) who did not include beam effects. The beam effect is shown in Fig. 2 where we plot the best-fitting carbon-rich model (with $t_1 = 9735$ yr and $t_2 = 1050$ yr) and the effect of the IRAS and JCMT beam.

We calculated the evolution in the IRAS color-color diagram for the carbon rich model with $t_1 = 9735$, $t_2 = 1050$ yr and the oxygen-rich model with $t_1 = 7620$, $t_2 = 1050$ yr. In Table 5 we list for the different models the times to reach $C_{32} = 2.5 \log(S_{60}/S_{25}) = -1.55$ which approximately separates groups II and III in Groenewegen et al. (1992). The lifetime depends on distance and expansion velocity like d/v. We conclude that the beam effect reduces the time scale to loop through the IRAS color-color diagram by 25–30%.

---

[2] The shell position of S Sct was observed on 29 and 31 october 1992 during a JCMT service observing run with the UKT 14 instrument. Upper limits of 25 mJy at 800 μm and 200 mJy at 450 μm were obtained.

References

Bergman P., Carlström U., Olofsson H., 1993, A&A 268, 685

Cardelli J.A., Clayton G.C., Mathis J.S., 1989, ApJ 345, 245

Chan S.J., Kwok S., 1988, ApJ 334, 362

Draine B.T., 1987, Princeton Observatory Preprint, 213, 1

Draine B.T., Lee H.M., 1984, ApJ 285, 89

Duncan W.D., Robson E.I., Ade P.A.R., Griffin M.J., Sandell G., 1990, MNRAS 243, 126

Egan M.P., Leung C.M., 1991, ApJ 383, 314

Frogel J.A., Persson S.E., Cohen J.G., 1980, ApJ 239, 495

Gillett F.C., Merrill K.M., Stein W.A., 1971, ApJ 164, 83

Groenewegen M.A.T., 1993, Ph.D. Thesis, Chap. 5, University of Amsterdam

Groenewegen M.A.T., de Jong T., van der Bliek N.S., Slijkhuis S., Willems F.J., 1992, A&A 253, 150

Hackwell J.A., 1972, A&A 21, 239

Hawkins G., 1992, in: Schwarz H. (ed.) Mass Loss on the AGB and Beyond (in press)

Joint IRAS Science Working Group, 1986, IRAS catalogs and atlases, Low Resolution Spectrograph (LRS), A&AS 65, 607

Joint IRAS Science Working Group, 1986, IRAS catalogs and atlases, Point Source Catalog (PSC), US Government Printing Office, Washington

Joint IRAS Science Working Group, 1986, IRAS catalogs and atlases, Explanatory Supplement, US Government Printing Office, Washington

de Jong, T., 1989, A&A 223, L23

Kholopov P.N., et al., 1985, General Catalog of Variable Stars. Nauka, Moscow

Knapp G.R., Morris M., 1985, ApJ 292, 640

Lambert D.L., Gustafsson B., Eriksson K., Hinkle K.H., 1986, ApJS 62, 373

Milne D.K., Aller L.H., 1980, AJ 85, 17

Neckel Th., Klare G., 1980, A&AS 42, 251

Ney E.P., Merrill K.M., 1980, The AFGL catalog, AFGL-TR-80-0050

Noguchi K., et al., 1981, PASJ 33, 373

Olofsson H., Carlström U., Eriksson K., Gustafsson B., 1992, A&A 253, L17 (OCEG)

Price S.D., Murdock T.L., 1983, The revised AFGL infrared sky survey catalog, AFGL-TR-83-0161

Rouleau F., Martin P.G., 1991, ApJ 377, 526

Rufener F., 1988, Catalog of stars measured in the Geneva photometric system, 4th edition, Observatoire de Geneva

Šleivyté J., 1987, Vilnius Astr. Obs. Bull. 77, 33

Sopka R.J., et al., 1985, ApJ 294, 242

Stephenson C.B., 1989, Publ. Warner and Swasey Obs., Vol. 3, No. 2

Vassiliadis E., Wood P.R., 1993, ApJ 413, 641

Volk K., Cohen M., 1989, AJ 98, 931

Walker A.R., 1979, South African Astron. Obs. Circ., Vol 1, No 4, 112

Walker A.R., 1980, MNRAS 190, 543

Willems F.J., 1988, A&A 203, 51

Willems F.J., de Jong T., 1988, A&A 196, 173

Yamamura I., Onaka T., Kamijo F., Izumiura H., Deguchi S., 1993, PASJ (YOKID) (in press)

Zijlstra A.A., Loup C., Waters L.B.F.M., de Jong T., 1992, A&A 265, L5

Zuckerman B., Maddalena R.J., 1989, A&A 223, L20